Nuclear Physics A535 (1991) 669–700
North-Holland

NUCLEAR
PHYSICS A

INTERPLAY BETWEEN SINGLE-PARTICLE AND COLLECTIVE DEGREES OF FREEDOM IN THE EXCITATION OF THE LOW-LYING STATES IN ^{142}Nd

R.K.J. SANDOR[1], H.P. BLOK[1], U. GARG[1,4], M.N. HARAKEH[1], C.W. DE JAGER[2], V.YU. PONOMAREV[3], A.I. VDOVIN[3] and H. DE VRIES[2]

[1] *Department of Physics and Astronomy, Vrije Universiteit, De Boelelaan 1081, 1081 HV Amsterdam, The Netherlands*

[2] *Nationaal Instituut voor Kernfysica en Hoge-Energie Fysica, Sectie K, P.O. Box 41882, 1009 DB Amsterdam, The Netherlands*

[3] *Laboratory of Theoretical Physics, Joint Institute for Nuclear Research Dubna, Head Post Office, P.O. Box 79, Moscow, USSR*

[4] *Physics Department, University of Notre Dame, Notre Dame, IN 46556, USA*

Received 3 April 1991
(Revised 14 June 1991)

Abstract: The low-lying excited states in ^{142}Nd were investigated by inelastic electron scattering. The momentum transfer range covered was 0.5–2.8 fm^{-1}. Transition charge densities were extracted for natural-parity states from 0^+ up to 9^- and up to an excitation energy of 3.5 MeV. For several new excited states spin and parity assignments have been suggested. The experimental transition charge densities have been interpreted with the aid of the quasiparticle-phonon model (QPM). The QPM is well-suited to investigate the contribution of collective and single-particle degrees of freedom to excited states in spherical nuclei. On the basis of the QPM calculations it is shown that in ^{142}Nd both degrees of freedom play an important role, as well as the interplay between them. Both the strength distribution and the structure of the transition charge densities of the low-lying excited states are well described by the calculations. The origin of the structure in the nuclear interior usually predicted by microscopic calculations but not observed experimentally is explained. An argument for the proton number dependence of the excitation energy of the 3_1^- state in the $N = 82$ isotones is given.

E

NUCLEAR REACTIONS ^{142}Nd(e, e'), $E = 112$–450 MeV; measured spectra; deduced longitudinal form factor of low-lying states. ^{142}Nd levels deduced L, J, π, transition charge densities, $B(\lambda)$ values. Fourier-Bessel analysis, microscopic quasiparticle-phonon model.

1. Introduction

With the availability of new, high resolution electron scattering facilities, the region of nuclei around the $N = 82$ neutron shell closure has regained interest. There are a few reasons for this: first, for a number of elements in the rare earth region the different isotopes display a shape transition from semi-magic, via vibrational to strongly deformed, rotational nuclei. This has been the subject of investigations in

the past and also recently a number of experiments to this purpose have been performed in Saclay [1,2]) (Sm isotopes), MIT-Bates [3]) (Ce isotopes) and NIKHEF-K (Nd isotopes). Second, it is possible to distinguish between different modes of excitation by looking at transition charge densities with a sensitive probe such as electron scattering.

In the present paper we will focus on this last aspect for the nucleus ^{142}Nd. There is evidence [4]) that in the $N=50$, $Z=40$ region the low-lying collective states are not only built of collective vibrations but also have considerable single-particle nature. As ^{142}Nd is a spherical nucleus with an $N=82$ closed neutron shell, excitations will involve mostly proton configurations, implying that the experimental transition densities will contain practically all nuclear structure information. Therefore, this nucleus is especially well suited to investigate the interplay between collective and single-particle degrees of freedom of low-lying excited states. The nucleus ^{142}Nd has also been the subject of recent studies with other experimental methods, such as inelastic proton scattering [5]) and low-energy photon scattering [6]).

The inelastic electron scattering experiments that will be discussed have been performed with the medium-energy accelerator MEA at NIKHEF-K. The excellent energy resolution made it possible to separate most states below an excitation energy of 3.6 MeV. Form factors, measured for effective momentum transfers from 0.5 up to 2.8 fm^{-1}, and transition charge densities, extracted from the form factors by means of Fourier-Bessel analysis, will be presented for natural parity states ranging from 0^+ up to 9^-. The densities have been compared to the results of calculations in the framework of the quasiparticle-phonon model (QPM), a model that has proven to be successful in describing a wide range of nuclear phenomena.

A preliminary report of this work on the low-lying quadrupole excitations has appeared earlier [7]). In this paper an extensive discussion of the data, for other multipolarities ranging from 0^+ up to $9^-$and the comparison with the calculations performed in the framework of the quasiparticle-phonon model (QPM) will be presented. To this end the paper is organized in the following way: in sect. 2 a description of the experimental setup and the data analysis is given and in sect. 3 a short outline of the QPM is described. In sect. 4 the experimental results for the 2^+, 3^-, 4^+ and other states, respectively, are presented and compared to the results obtained from the calculations. The conclusions are given in sect. 5.

2. Experimental procedures and data analysis

2.1. EXPERIMENTAL PROCEDURES

The experiment was performed at the electron scattering facility of the NIKHEF-K. Detailed information about the accelerator, the beam transport, the spectrometer and the detection system is available in ref. [8]). Only system properties especially relevant to the present work are to be discussed in this subsection.

The beam is produced by the medium energy accelerator (MEA). The resolution in energy is 0.2%. To improve on this resolution for the detected electrons, the beam is led through the beam handling system (BHS), which is tuned in such a way that the dispersion of the beam on the target matches that of the spectrometer. The spectrometer used in the present experiment is the QDD spectrometer, which is designed to combine a good energy resolution ($\leq 1 \times 10^{-4}$) with a large solid angle (5.6 msr). The detection system of the QDD spectrometer [9]) consists of a stack of four multiwire drift chambers (MWDC), triggered by a set of scintillators and Çerenkov counters. Two MWDCs measure the position and direction of the scattered electron in the dispersive plane and two in the non-dispersive plane, making it possible to reconstruct the trajectory of each event through the spectrometer [10]). This allows, with the knowledge of the magnetic field, the determination of the scattering vector of the electron at the target. Therefore, by taking data on an event-by-event basis one is able to correct for spectrometer aberrations and kinematic broadening in the off-line analysis. In this data-taking mode one is limited to approximately 900 counts per second. Therefore, if the count rates were higher, as was the case for the lowest q-values, the data were acquired on-line in spectral form (spectrum mode). The loss in resolution for these data was nonetheless small, since a small spectrometer opening slit was used. The collected charge is measured by means of a toroid monitor.

The ^{142}Nd target of a thickness of 10.2 mg/cm^2 was obtained by reducing, melting and rolling enriched Nd_2O_3 powder. The target thickness was chosen as a compromise between count rate and resolution. A (p, p') experiment was performed to determine the isotopical purity of the target material, which turned out to be 99%. The inhomogeneities of the target were estimated to be less than 1%. For optimum resolution the target was set in transmission mode.

The data were taken over an effective transferred momentum range from 0.5 to 2.8 fm^{-1} in steps of approximately 0.15 fm^{-1}. The effective tranferred momentum is defined as

$$q_{\text{eff}} = q(1 + \tfrac{3}{2} Z\alpha / E_i R_{\text{eq}}) , \tag{1}$$

where α is the fine structure constant, R_{eq} is the equivalent radius of a homogeneously charge sphere containing the nuclear charge, commonly taken to be $1.12A^{1/3}$. This range was large enough to permit a model-independent analysis of the measured form factors to obtain transition densities. The choice of angles and energies was governed on the one hand by the necessity of achieving as good a resolution as possible and, on the other hand, by the desirability of minimizing the contribution of the transverse form factors, thus limiting the maximum scattering angle. The final data set was comprised of beam energies between 112 and 450 MeV with an energy resolution of 12 keV up to 30 keV. Two solid-angle defining slits were used, a small one with an acceptance of 0.4 msr and a large one with an acceptance of 5.6 msr. Correction for the dead-time losses was made by multiplying the contents of each

spectrum with the factor $\tau = N_p/N_c$ with N_p being the number of triggers of the scintillators and N_c being the number of triggers accepted by the whole detection system. The relative wire efficiencies were extracted from additional mesurements. More information on dead-time losses and relative wire efficiencies can be found in ref. [11]).

Since the energy of the incoming beam is only approximately known, a calibration was performed for each energy according to the usual method by recoil energy differences. An additional run on a natural boron-nitride target was performed for this purpose. These data were then simultaneously used to calibrate the excitation energy scale along the focal plane [12]).

To extract the cross sections from the measured spectra, the number of counts in each peak was determined by means of a lineshape-fitting procedure. To this end the program ALLFIT [13]) was used, which corrects for straggling, bremsstrahlung and Schwinger effects [14]). In the fitting procedure no background was used, except for the data taken in spectrum mode, where a (small) flat background was assumed. In this way form factors for 17 states up to an excitation energy of 3.6 MeV were extracted. Fig. 1 shows, as an example, a fitted spectrum for ^{142}Nd, taken at $E_i = 243.5$ MeV and $\theta = 40.25°$ corresponding to a q_{eff} of 1.1 fm^{-1}.

The efficiency of the detector system was checked before most measurements by a run on ^{12}C. These runs were also used to eliminate some of the systematic errors in the cross sections. To this end the cross sections for the 0^+ ground state of ^{12}C at each energy-angle combination of the experiment were calculated from the

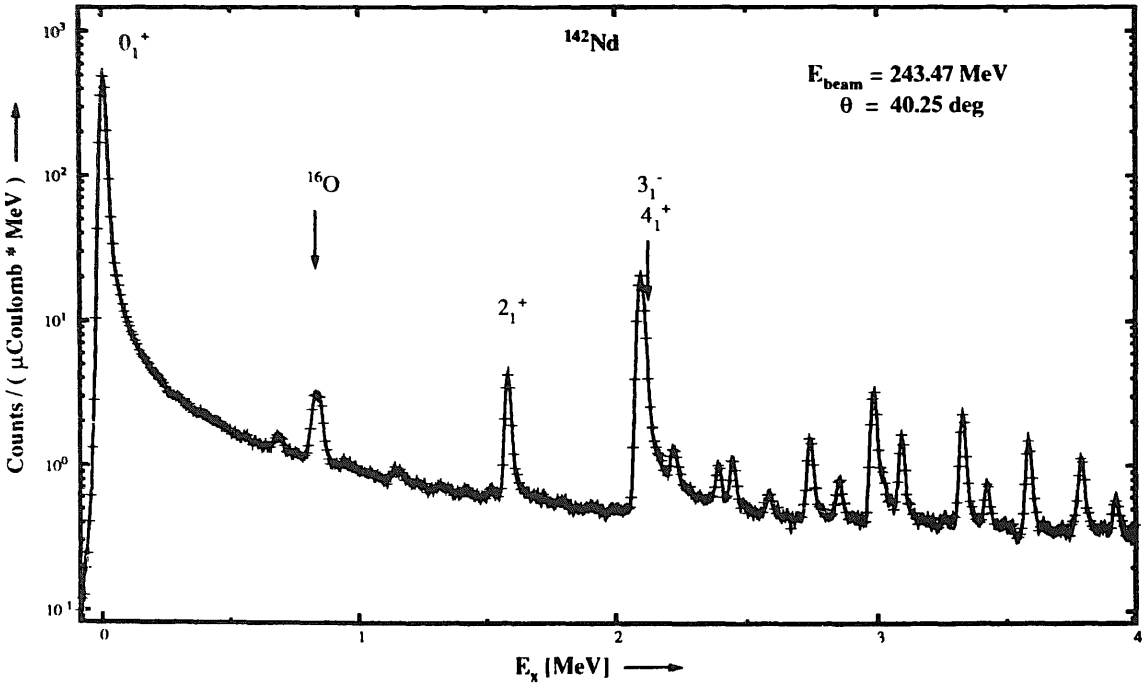

Fig. 1. Fitted spectrum for ^{142}Nd at a transferred momentum of $q_{eff} = 1.1$ fm^{-1}. The peak due to the target contaminant ^{16}O as well as the spin and parities of some of the strongest excitations are marked.

accurately known charge distribution [15]). The ratio between the calculated and the measured cross sections thus was a measure for the absolute efficiency of the detection system, under the assumption that the conditions during the carbon run were the same as for the neodymium runs. It was always found to be better than 98% after correction for the wire-chamber efficiencies. This procedure could not be applied in the vicinity of the very steep form factor minimum at $q = 1.7$ fm^{-1} of the ground state of ^{12}C. At some other q-values there was either no carbon measurement performed or the quality of it was such, that it could not be used for normalization purposes. These runs therefore have a larger systematic error.

For each data point statistical errors due to a number of sources were added quadratically to the statistical error in the cross section. In the case of elastic scattering the shape of the form factor as a function of the scattering angle and the beam energy was taken into account in the determination of the errors in the cross sections. This has not been done for inelastic scattering to excited states. Instead, an additional statistical error of 2.5% was used. The systematic errors which could not be eliminated in the normalization procedure were then summed linearly to the total statistical error.

2.2. FOURIER-BESSEL ANALYSIS

In order to obtain transition charge densities from the measured form factors a Fourier-Bessel analysis was performed according to the parametrization of Heisenberg [16,17]). In this parametrization the transition charge densities are expanded in a series of Bessel functions up to a cut-off radius R_c beyond which the charge density is assumed to be zero.

In principle this procedure is model-independent, since these expansions are complete. However, as the measured data extend only up to a maximum transferred momentum q_{max} of 2.8 fm^{-1}, a certain form factor behaviour beyond this point has to be assumed. To this end the prescription of Rothhaas *et al.* [18]) was used, specifying an "upper limit" beyond q_{max}, given by an exponentially decreasing function, that gives a reasonable envelope to the lower-momentum data. The limit was enforced through the use of pseudo-data. These data were of zero cross section with error bars given by the upper limit envelope. With this procedure 15 Fourier-Bessel coefficients have been fitted. The inclusion of the pseudo-data in the fit then yields the model or incompleteness error.

Furthermore, a cut-off R_c of 11.5 fm was chosen. This is a normal value for this mass region and is a compromise between having a reasonable number of parameters and avoiding unphysical oscillations far outside the nucleus. In view of the latter problem also a constraint in r-space was used, a so-called tail bias [16]). A tail bias is a restriction which assumes that beyond a certain R_t the transition charge distribution falls off like some function of r. This function is chosen, in accordance with the radial dependence of the wave function of the least bound nucleon(s), to

have the shape of a Whittaker function [19]). Hence, the overlap at large radii between the wave function of the initial state and that of the final state is taken as

$$\rho(r) \sim e^{-\beta r}. \tag{2}$$

A variance is then defined as a pseduo-χ^2 given by

$$\chi^2 = \sum_i \left[\frac{\rho(r_i) - \rho(R_1)\, e^{-\beta(r_i - R_1)}}{P} \right]^2. \tag{3}$$

P is the weight factor of the tail constraint. It was chosen, together with R_1, for each transition charge density separately so as to give the most acceptable shape. The number i was determined by taking an equidistant distribution of pseudo-data between R_1 and R_c with a spacing of 0.2 fm.

3. The quasiparticle–phonon model

In this section a description of the quasiparticle-phonon model (QPM) is presented for even-even spherical nuclei. the main idea of the QPM is to construct a *phonon basis*, whereby phonons are defined as solutions of the quasiparticle-RPA equations. The phonon basis is then used to calculate two- and multiple-phonon states, which are subsequently coupled to the one-phonon states to obtain the spectrum of excited states. The goal of the model is to be able to describe the interplay between collective and single-particle degrees of freedom in the excitation of low-lying excited states in spherical nuclei. Of interest for the present work are of course the calculated transition charge densities, which can directly be compared to the experimental transition charge densities.

Detailed information about aspects of the QPM which will not be treated in this work, such as the description of giant resonances and properties of odd nuclei in a wide range of excitation energies can be found in refs. [20–22]).

3.1. GENERAL FORMALISM

The QPM uses an effective hamiltonian which consists of four parts:

$$H = H_{\rm sp} + H_{\rm pair} + H_{\rm m} + H_{\rm sm}, \tag{4}$$

where $H_{\rm sp}$ is the single-particle hamiltonian, $H_{\rm pair}$ represents the monopole pairing interaction, $H_{\rm m}$ is the separable multipole interaction in the ph channel, and $H_{\rm sm}$ is the separable spin-multipole interaction in the ph channel.

First, a spectrum of excited states is calculated. This is done in the BCS approximation. In this approximation the particle creation and annihilation operators a^+_{jm} and a_{jm} are transformed into quasiparticle operators. The coefficients u_j and v_j of the Bogoliubov transformation are chosen to minimize the expectation value of the

operator $H_{sqp} = H_{sp} + H_{pair}$ for the quasiparticle vacuum $|0\rangle$. In this way the operator H_{sqp} takes the form

$$H_{sqp} = \sum_{jm}^{N} E_j \alpha_{jm}^{+} \alpha_{jm} + \sum_{jm}^{Z} E_j \alpha_{jm}^{+} \alpha_{jm}, \tag{5}$$

where the energy of the quasiparticle $|jm\rangle$ is

$$E_j = [(\varepsilon_j - \lambda_\tau)^2 + C_\tau^2]^{1/2}. \tag{6}$$

Here, λ denotes the chemical potential, τ the isospin of the quasiparticle and C_τ the correlation function (energy gap).

Next, a two-quasiparticle creation operator A^+ is defined in the following way:

$$A^+(jj'\lambda\mu) = \sum_{mm'} \langle jmj'm' | \lambda\mu \rangle \alpha_{jm}^{+} \alpha_{j'm'}^{+}. \tag{7}$$

and a unitary transformation from the operators $A^+(jj'\lambda\mu)$ and $A(jj'\lambda\mu)$ to phonon creation and annihilation operators $Q_{\lambda\mu i}^{+}$ and $Q_{\lambda\mu i}$ is performed:

$$Q_{\lambda\mu i}^{+} = \tfrac{1}{2} \sum_{jj'}^{N,Z} [\psi_{jj'}^{\lambda i} A^+(jj'\lambda\mu) + (-1)^{\lambda-\mu} \phi_{jj'}^{\lambda i} A(jj'\lambda - \mu)]. \tag{8}$$

The phonons defined in this way represent both pure two-quasiparticle excitations and collective excitations, to the structure of which many two-quasiparticle configurations contribute.

To obtain a basis of phonons, the amplitudes $\psi_{jj'}^{\lambda i}$ and $\phi_{jj'}^{\lambda i}$ are calculated. This is done by solving the so-called quasiparticle-RPA equations for each J^π, which follow from the ansatz that the hamiltonian $\hat{H} = H_{qsp} + H_{res}$ is approximately that of a set of independent harmonic oscillators of which $Q_{\lambda\mu i}^{+}$ are the creation operators of an oscillator quantum phonon with energy $\omega_{\lambda i}$:

$$[\hat{H}, Q_{\lambda\mu i}^{+}] = \omega_{\lambda i} Q_{\lambda\mu i}^{+}. \tag{9}$$

It can be easily shown that this leads to vibrational ph excitations superposed on a ground state, which is defined as a phonon vacuum, i.e. $Q_\mu |\mathrm{RPA}\rangle = 0$. The approximation (9), in which more complicated terms on the right-hand side have been neglected by assuming that they occur with random signs (phases), leads to coupled equations for the amplitudes ψ and ϕ, the RPA equations.

One of the main features of defining phonons as in eq. (8) is that by applying the phonon creation operator to the $|\mathrm{RPA}\rangle$ ground-state wave function one can not only create a quasiparticle pair, but also destroy one, meaning that it is possible to deal with two-quasiparticle correlations in the ground state. The RPA equations yield also the excitation energies $\omega_{\lambda i}$, where λ denotes the angular momentum and i the root number of the solution. The expressions for $\omega_{\lambda i}$, $\psi_{jj'}^{\lambda i}$ and $\phi_{jj'}^{\lambda i}$ in RPA can be found in ref. [23]).

With the obtained phonon basis the hamiltonian (4) can be rewritten in terms of phonon operators:

$$H = \sum_{\lambda\mu i} \omega_{\lambda i} Q^{+}_{\lambda\mu i} Q_{\lambda\mu i} + \frac{1}{2\sqrt{2}} \sum_{\lambda\mu i} \sum_{\substack{\lambda'\mu' i' \\ \lambda''\mu'' i''}} \{ U^{\lambda'' i''}_{\lambda' i'}(\lambda i) [[Q^{+}_{\lambda'\mu' i'} Q^{+}_{\lambda''\mu'' i''}]_{\lambda\mu} Q_{\lambda\mu i}]_{00} + \text{h.c.} \} + \cdots , \tag{10}$$

where the square brackets indicate angular momentum coupling. The wave functions then have the following form:

$$\Psi_v(JM) = \left\{ \sum_i R_i(Jv) Q^{+}_{JMi} + \sum_{\substack{\lambda\mu i \\ \lambda'\mu' i'}} P^{\lambda' i'}_{\lambda i}(Jv) [Q^{+}_{\lambda\mu i} Q^{+}_{\lambda'\mu' i'}]_{JM} \right\} \Psi_{\text{g.s.}}$$

$$+ \left\{ \sum_{\substack{\lambda\mu i \\ \lambda'\mu' i'}} \sum_{\substack{J' \\ \lambda''\mu'' i''}} T^{J'\lambda'' i''}_{\lambda i \lambda' i'}(Jv) [[Q^{+}_{\lambda\mu i} Q^{+}_{\lambda'\mu' i'}]_{J'M'} Q^{+}_{\lambda''\mu'' i''}]_{JM} + \cdots \right\} \Psi_{\text{g.s.}} \tag{11}$$

The first term of eq. (10) corresponds to the non-interactive phonon approximation, whereas the second describes the interaction between the different parts of the wave function (11) with the exchange of one phonon. Terms involving the exchange of three, five, ... phonons are not shown. The matrix element $U^{\lambda' i'}_{\lambda'' i''}(\lambda i)$ of the interaction between one- and two-phonon components of the wave function is a function of the phonon amplitudes $\psi^{\lambda i}_{jj'}$ and $\phi^{\lambda i}_{jj'}$ and the matrix element of the residual interaction. Their precise relation can be found in ref. [24]).

The transformation from quasiparticles to phonons leads to a violation of the Pauli principle. As phonons are integer-spin configurations, they obey Bose statistics and thus the underlying physical property of nucleons being fermions is ignored. The consequences are twofold: first, the total many-phonon basis is overdetermined compared to the correctly antisymmetrized many-quasiparticle basis. Second, the violation of the Pauli principle necessitates a renormalization of the matrix elements of the quasiparticle-phonon interaction $\psi^{\lambda i}_{jj'}$ and $\phi^{\lambda i}_{jj'}$. It has been shown in ref. [22]) that for even-even spherical nuclei the first consequence is the most important, leading to many spurious states. In the present work the Pauli principle was taken into account in the *diagonalization approximation* (for details see refs. [23-25])), which has proven to be sufficient for the present type of calculations while rigorously simplifying the calculations.

3.2. TRANSITION DENSITIES

In the present calculations the wave functions (11) for excited states with up to three phonons were included. Diagonalizing the hamiltonian (10) results in the excitation energies of excited states η_{Jv} (v is the root number) and the structure coefficients R, P and T. With these quantities transition charge densities can be

calculated. If one neglects ground-state correlations, only one-phonon $\rho_i^J(r)$ and two-phonon $\rho^J_{\lambda i\lambda' i'}(r)$ densities contribute to the transition charge densities $\rho_v^J(r)$:

$$\rho_v^J(r) = \sum_i R_i(Jv)\rho_i^J(r) + \sum_{\lambda i\lambda' i'} P^{\lambda' i'}_{\lambda i}(Jv)\rho^J_{\lambda i\lambda' i'}(r) \tag{12}$$

with

$$\rho_i^J(r) = \sum_{j'}^{N,Z} \tfrac{1}{2}\rho^J_{jj'}(r)u^{(+)}_{jj'}(\psi^{Ji}_{jj'} + \phi^{Ji}_{jj'}) \tag{13}$$

and

$$\rho^J_{\lambda i\lambda' i'}(r) = -\sum_{jj'j''}^{N,Z} \rho^J_{jj'}(r)v^{(-)}_{jj'}\hat{\lambda}\hat{\lambda}' \begin{Bmatrix} \lambda & \lambda' & J \\ j & j' & j'' \end{Bmatrix} (\psi^{\lambda i}_{j'j''}\phi^{\lambda' i'}_{j''j} + \phi^{\lambda i}_{j'j''}\psi^{\lambda' i'}_{j''j}) . \tag{14}$$

In these formulas

$$\hat{\lambda} = \sqrt{2\lambda + 1} \tag{15}$$

and the two-quasiparticle transition charge densities $\rho^J_{jj'}(r)$ have the form [26])

$$\rho^J_{jj'}(r) = (-1)^{j-1/2} i^{l'-l-J} \frac{\hat{j}\hat{j}'}{4\hat{J}\sqrt{\pi}} (1 + (-1)^{l+l'+J}) e_\tau \langle j\tfrac{1}{2} j' - \tfrac{1}{2} | J0\rangle u_j^*(r)u_{j'}(r) , \tag{16}$$

where $u^{(+)}_{jj'} = u_j v_{j'} + u_{j'} v_j$ and $v^{(-)}_{jj'} = u_j u_{j'} - v_{j'} v_j$ are combinations of the Bogoliubov transformation; $u_j(r)$ is the radial part of the single-particle wave function and e_τ is the effective charge of the nucleon. Finally, to compare the calculated transition charge densities with those obtained from the experiment, the $\rho_v^J(r)$ are folded with the proton form factor, which is parametrized according to ref. [27]).

The different parameters in the calculations are determined in the following ways. For the single-particle part of the hamiltonian (4) a Saxon-Woods potential has been used with the radial parameters for protons taken from ref. [28]) ($r_0 = 1.30$ fm, $a_0 = 0.55$ fm) and for neutrons from ref. [29]) ($r_0 = 1.27$ fm, $a_0 = 0.62$ fm). All bound and narrow quasi-bound states so obtained were included in the calculations, making a total of 28 neutron levels and 29 proton levels with $j \leq \frac{19}{2}$. With this single-particle spectrum the model-independent energy-weighted sum rule [30]) is reproduced for low J^π. Therefore, no effective charges are thought to be necessary: $e_Z = 1$ and $e_N = 0$. Only for the $J^\pi = 1^-$ states different values are used to remove spurious motion of the center of mass: $e_Z = N/A$ and $e_N = -Z/A$.

Pairing correlations are treated in the BCS approximation with a constant value for the matrix element of the monopole pairing interaction in the particle-particle channel. It is chosen to reproduce the odd-even mass difference of neighbouring isotones.

For the residual interaction a separable multipole interaction in the particle-hole channel is used. The radial dependence of the forces is taken to be the derivative of the central part of the Saxon-Woods potential. For each multipolarity the

parameters of the effective residual forces are chosen to reproduce the experimental excitation energy of the lowest state and the obtained values $\kappa_{0,1}^{J^\pi}$ for different J^π are close together. In this procedure the strength ratio of the isovector force to isoscalar force is kept constant at $\kappa_1^{J^\pi}/\kappa_0^{J^\pi} = -1.2$.

All one-phonon configurations with energies $E_x \leq 4.5$ MeV and two-phonon configurations with $E_x \leq 6.5$ MeV are included in the calculations. Moreover, all important three-phonon configurations involving the 2_1^+, 3_1^- and 4_1^+ one-phonon terms have also been taken into account in the wave function. It should be remarked, that after the definition of the phonon basis, no further free parameters are introduced in the description of the interaction between phonons.

4. Comparison between the experimental data and the calculations

In this section the comparison between the experimental data and the theoretical calculations will be presented. Table 1 lists the excitation energies and the multipolarities for the levels observed in the present experiment, compared to a compilation of previous experiments [5,31,32]).

TABLE 1

List of measured excitation energies with statistical errors in comparison to a compilation of the Nuclear Data Sheets [31]), the work of Trache *et al.* [5]) and the preliminary results of Pignanelli *et al.* [32]). Energies of states which could not be measured accurately enough are given without errors

Literature		Present work		Literature		Present work	
E_x (MeV)	J^π	E_x (MeV)	J^π	E_x (MeV)	J^π	E_x (MeV)	J^π
1.5768	2^+	1.575 (4)	2^+	3.0457	2^+ [a])	3.045	
2.0844	3^-	2.083 (6)	3^-	3.080	(4^+) [a])	3.080 (7)	4^+
2.0989	4^+	2.098	4^+	3.1281	$(1, 2^+)$	3.135	
2.2073	$(6)^+$	2.21 (4)	6^+	3.151			
2.2172	0^+			3.2429	$(7)^-$	3.246 (6)	7^-
2.340				3.244	$(4)^-$		
2.3843	2^+	2.385 (8)	2^+	3.295	$(4)^-$		
2.438 [a])	(4^+) [b])	2.438 (20)	4^+	3.300	$(2, 3)^+$		
2.550	$(3, 2)^+$			3.311	(4^+) [a])	3.319 (8)	4^+
2.5833	$1(^+), 2^+$	2.584 (18)	(4^+)	3.358	$(2, 1)^+$		
2.739 [a])		2.739 (12)	5^-	3.366	$(3)^-$		
2.8459	2^+	2.845 (6)	2^+	3.413	$(5)^-$	3.413 (12)	(6^+)
		2.893	(6^+)	3.425 [c])	1^- [c])		
2.956				3.453	(8)		
2.978	0^+	2.976 (6)	0^+	$3.456 + x$	$(9)^-$	3.494 (9)	(9^-)
3.008		3.008		3.563	3^- [a])	3.580 (16)	3^-

[a]) From Trache *et al.* [5]).
[b]) From Pignanelli *et al.* [32]).
[c]) From Pitz *et al.* [6]).

A preliminary analysis of the quadrupole states has been given in an earlier paper [7]). Since then the data have been reanalyzed and the parameters of the Saxon-Woods potential used in the QPM have been adjusted to the values obtained from an exclusive (e, e'p) experiment on ^{142}Nd performed at NIKHEF-K by Lanen *et al.* [28])

4.1. THE QUADRUPOLE STATES

The quasiparticle-RPA predicts six quadrupole one-phonon states below 4 MeV. Their excitation energies and B(E2) values are lised in table 2 and the calculated transition charge densities of the lowest four states are shown in fig. 2. As ^{142}Nd has a closed neutron shell, the pairing correlations in the neutron system vanish. This leads to the first neutron particle-hole 2^+ configuration having an energy higher than 5 MeV. Consequently, proton components dominate the states of table 2. The 2_1^+ one-phonon state is the most collective. The 2_2^+ and 2_3^+ states have, as to be expected, much smaller B(E2) values. However, the 2_4^+ state is again very collective, its B(E2) value being only three times smaller than that of the 2_1^+ state. This behaviour of collective versus non-collective is reflected in the transition charge densities. Both the transition charge densities of the 2_1^+ and 2_4^+ states peak mainly at the nuclear surface, whereas those of the 2_2^+ and 2_3^+ states have very pronounced volume peaks. A possible explanation lies in the single-particle subshell-structure, shown in fig. 3a. The two proton subshells $1g_{7/2}$ and $2d_{5/2}$ are close together and close to the Fermi level, whereas other proton subshells, notably the $1h_{11/2}$, $2d_{3/2}$ and $3s_{1/2}$ have about 2 MeV higher single-particle energies. This results in about 1 MeV higher quasi-particle energies for these levels than for the $1g_{7/2}$ and $2d_{5/2}$ subshells, as can

TABLE 2

Excitation energies and B(E2) values of the quadrupole states observed in this experiment compared to those from the QPM calculations. The results of the RPA calculations and those of the full calculations after coupling the two- and three-phonon states are listed

J^π	v	Calculation				Experiment	
		RPA		QPM			
		E_x (MeV)	B(E2) (e^2 fm^4)	E_x (MeV)	B(E2) (e^3 fm^4)	E_x (MeV)	B(E2) (e^2 fm^4)
2^+	1	1.900	3816	1.630	4060	1.575	2810 (10) [a])
	2	2.480	124	2.420	247	2.385	309 (17)
	3	2.600	269	2.530	173		
	4	3.300	1327	3.050	705	2.845	498 (20)
	5	3.830	3.3	3.320	99	3.045	
	6	3.940	0.5	3.920	40		

[a]) The B(E2) value has been taken from ref. [31]) and used in the Fourier-Bessel analysis as a data point.

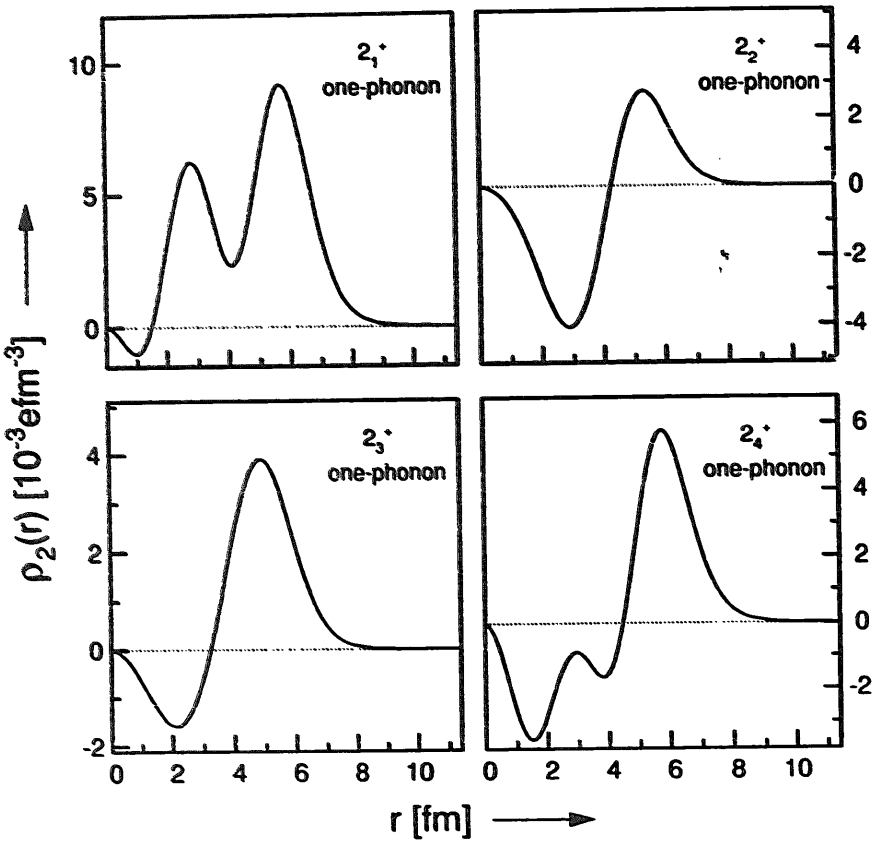

Fig. 2. Transition charge densities resulting from the RPA calculations for the first four 2^+ one-phonon states in ^{142}Nd.

also be seen in fig. 3. This is also observed in the adjacent odd nuclei. The 2_4^+ state is mainly built from many different configurations involving the orbits higher in energy and due to the gap is much more collective than the almost pure two-quasiparticle 2_2^+ and 2_3^+ states.

After coupling the one-, two- and three-phonon configurations, one obtains again six 2^+ states below 4 MeV, listed in table 2. The coupling between the one-phonon configurations and the two-phonon configurations is not very strong and the traces of three-phonon terms are not seen up to 3.0 MeV. This is usual for semi-magic nuclei [33]). The first quadrupole $[2_1^+ \times 2_1^+]$ two-phonon state is located rather high ($E_x = 3.8$ MeV), and other two-phonon states lie even higher still ($E_x > 4$ MeV). Therefore, the (collective and non-collective) one-phonon components dominate in the wave functions of the 2^+ states below 3 MeV. Indeed, the admixtures of the two-phonon components do not exceed a few percent for the lowest four 2^+ states. Because the densities of the two-phonon transitions as a rule [34]) are faded over the nuclear interior and their strengths are small (see also fig. 4), the contribution of the two-phonon admixtures to the transition charge densities is hardly visible. More important is the mixing of the different one-phonon components and their renormalization due to the two-phonon part of the wave function as a whole. In fig. 5

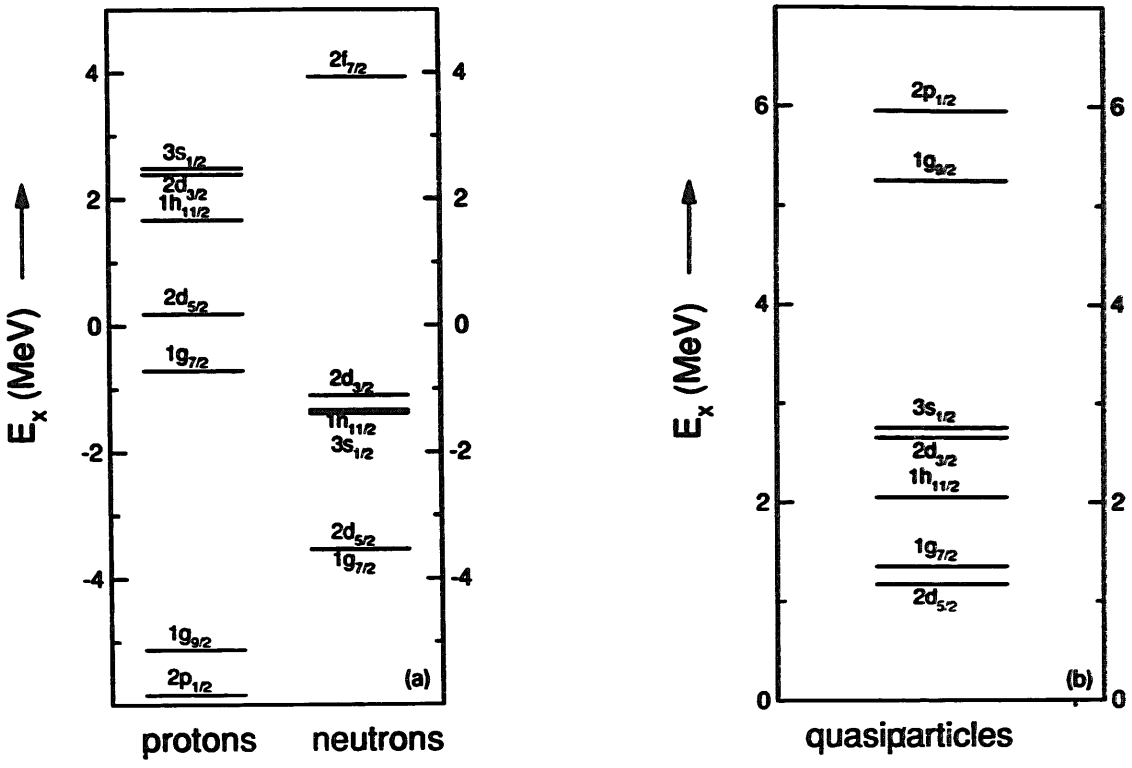

Fig. 3. (a) Single-particle spectrum of ^{142}Nd in the vicinity of the Fermi level, (b) quasiparticle spectrum of ^{142}Nd up to an excitation energy of 7 MeV.

the calculated transition charge densities for the lowest three observed quadrupole states are compared with the experimental data. The theoretical excitation energies and transition probabilities are summarized in table 2.

The systematics of the excitation energies of the quadrupole states are well reproduced. However, the spacing between the states is slightly overestimated by

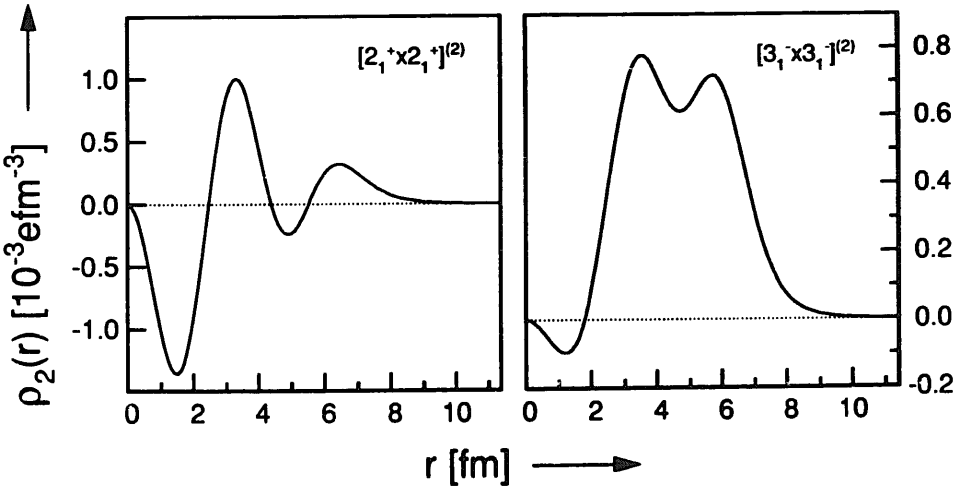

Fig. 4. Transition charge densities of the $[2_1^+ \times 2_1^+]^{(2)}$ and $[3_1^- \times 3_1^-]^{(2)}$ two-phonon states, calculated in the QPM.

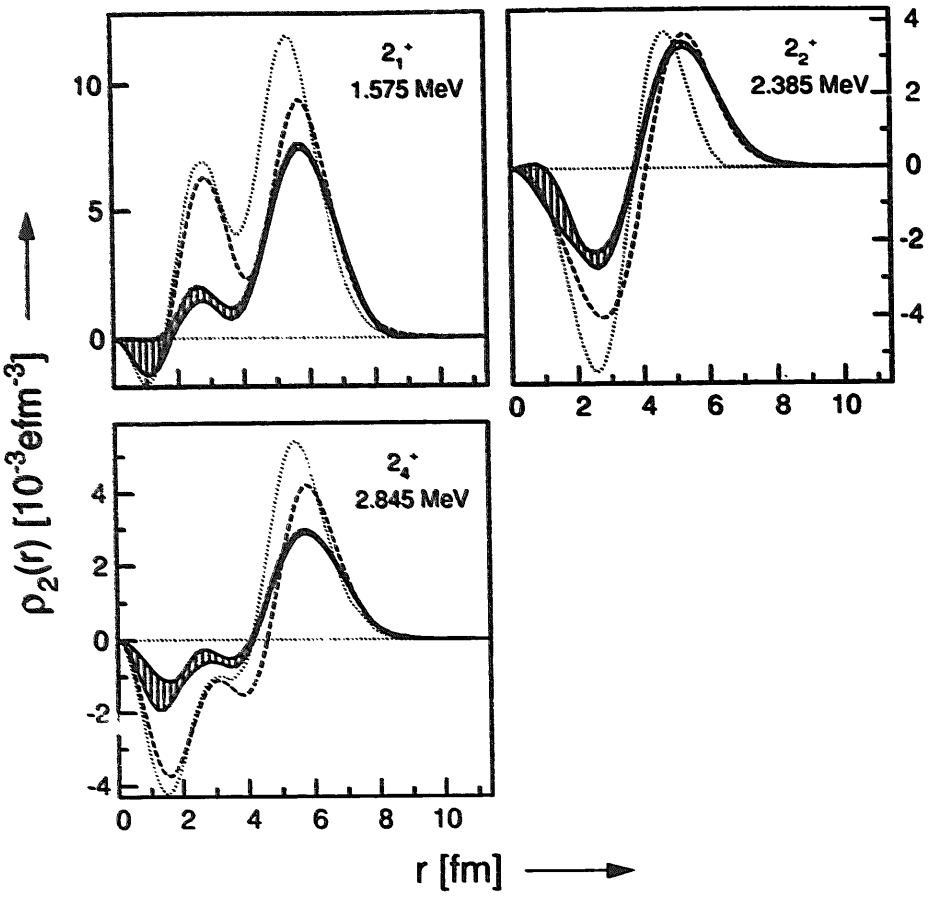

Fig. 5. The experimental transition charge densities (curves with error bands) compared with the QPM calculations (dashed lines) for the quadrupole states at respectively 1.575, 2.385 and 2.845 MeV in ^{142}Nd. Also shown (dotted lines) are the results from the QPM calculations with the old Saxon-Woods parameters, published earlier [7]).

the calculations. It is worth noting that the agreement in case of the 2_1^+ state is due to the adjustment of the strength of the multipole term to reproduce its excitation energy. The transition charge densities for the 2_1^+ and 2_4^+ states are clearly dominated by the respective one-phonon components. Indeed, other components contribute separately only below the 1% level, adding up to a total of 10%. This is not the case for the 2_2^+ and the 2_3^+ states. Here the coupling to the two-phonon states leads to a considerable mixing of the second and the third one-phonon states on the 10% level. As a result the B(E2) value of the 2_2^+ state increases, whereas that of the 2_3^+ state decreases due to destructive interference. This probably explains why this state is not detected in the present experiment. Indeed, if the calculated transition charge density of the 2_3^+ state is used to calculate a form factor, the cross sections are well within the error bars of the radiative tails of the stronger peaks with lower excitation energies. However, a state at 2.550 MeV has been reported [35]), which is believed to be a possible 2^+ state.

Quite remarkable is the measured and predicted high collectivity of the 2_4^+ state. This is evidence of the already mentioned gap in the proton single-particle spectrum

$(1g_{7/2}, 2d_{5/2} \Leftrightarrow 1h_{11/2}, 3s_{1/2}, 2d_{3/2})$. Generally, all three measured transition charge densities are reasonably reproduced by the calculations. As a consequence of the adjusted parameters of the Saxon-Woods potential the positions of the calculated surface maxima are now in agreement with the data in contrast to our preliminary publication [7]), in which a Saxon-Woods potential with $r_0 = 1.24$ fm and $a = 0.65$ fm was used.

A striking feature is, that the calculations overestimate the observed structure in the nuclear interior. This interior structure is also seen in the RPA one-phonon transition charge densities and can be traced back to a too large contribution of the $(2d_{5/2})^2$ two-quasiparticle component. This has an even larger influence on the calculated transitions charge densities of the hexadecapole states. Therefore, the discussion of this effect will be left to the section dealing with the 4^+ states.

It is interesting to note that the B(E2) value for the 2_1^+ state from the RPA calculations is about 30% larger than the experimental value. This is in contrast to the usually too small B(E2) value resulting from microscopic calculations with a truncated basis. Coupling to one- and multiple-phonon states even leads to an increase of the strength of the 2_1^+ state. This may be attributed to a depletion of strength from the giant quadrupole resonance (GQR). Although the states that build the resonance are included in the single-particle basis, the one-phonon states from the resonance region are not included in the wave functions of excited states, since the one-phonon basis is cut at an excitation energy of $E_x = 4.5$ MeV, well below the resonance. Therefore, the coupling of the 2_1^+ state with the GQR is not fully taken into account.

At higher excitation energies no 2^+ states were identified in the present experiment, although the calculations predict another state at approximately 3.32 MeV. Indeed, in a (p, p') experiment on ^{142}Nd [ref. [5])] a quadrupole state at 3.040 MeV has been identified with an isoscalar transition strength of about a factor five smaller than that of the 2_4^+ state. This strength is in agreement with the calculation and also explains why this state is hardly seen in the present experiment except for the q-region between 1.0 and 2.0 fm^{-1}, where a peak at 3.045 MeV was observed. A transition density for this state could therefore not be extracted.

4.2. OCTUPOLE STATES

Two 3^- one-phonon states are calculated below 4 MeV by the quasiparticle RPA. The excitation energies and B(E3) values are listed in table 3. Again, as for the quadrupole excitations, only proton configurations contribute. The first 3^- one-phonon state is very collective in contrast to the second one, which has a more or less pure two-quasiparticle configuration and consequently has a predicted transition strength of about two orders of magnitude smaller.

An interesting feature of the first octupole state in the even $N = 82$ isotones from ^{138}Ba to ^{144}Sm is the strong dependence of the excitation energy on the proton number, whereas the excitation energies of the 2_1^+ and 4_1^+ states remain practically

TABLE 3

Excitation energies and B(E3) values of the octupole states observed in this experiment compared to those from the QPM calculations. The results of the RPA calculations and those of the full calculations after coupling the two- and three-phonon states are listed

J^π	ν	Calculation				Experiment	
		RPA		QPM			
		E_x (MeV)	B(E3) (e^2 fm^6)	E_x (MeV)	B(E3) (e^2 fm^6)	E_x (MeV)	B(E3) (e^2 fm^6)
3^-	1	2.500	20.0×10^4	2.050	18.5×10^4	2.083	$26.20(15)\times10^4$
	2	3.370	0.11×10^4	3.280	0.23×10^4		
	3	4.831	5.37×10^4	4.010	1.32×10^4	3.580	1×10^4 [a]
	4			4.710	4.04×10^4		

[a] Obtained using a standard density with a maximum at $r = 5.5$ fm.

constant. This feature is illustrated in fig. 6a. An indication of the origin of this feature can be obtained by looking at the main two-quasiparticle configurations contributing to the respective excitations in ^{142}Nd. Whereas the 2_1^+ and 4_1^+ one-phonon states are built mainly of excitations within a subshell, in case of the 3_1^- state two quasiparticle levels are involved. Consequently one may expect that the excitation energy of the 3_1^- state will vary more strongly as a result of the difference between the energies of the contributing quasiparticles levels than that of the 2_1^+ and 4_1^+ states. In order to study this proton number dependence, quasiparticle BCS calculations were performed for the even $N = 82$ isotones, in which all parameters were kept fixed to the values used in the calculations for ^{142}Nd and just the proton number was varied. The resulting energies of the quasiparticle levels are depicted in fig. 6b. It is clear that the difference in energy of the $2d_{5/2}$ and $1h_{11/2}$ quasiparticle levels, which form the main quasiparticle configuration contributing to the first octupole one-phonon state, decreases by a factor of two in going from ^{138}Ba to ^{144}Sm, thus indicating the sensitivity of the excitation energy of the 3_1^- state to shell effects. Although the presented argument about one-phonon states of course cannot be applied to the description of real excitations, a full QPM calculation, performed without adjusting the multipole strength parameters of the residual interaction, reproduces the systematics of the excitation energy of the 3_1^- state [36].

After coupling the one- and two-phonon states one obtains the octupole states listed in table 3. As can be seen, only three states have an excitation energy lower than 4.1 MeV. The 3_1^- state is quite collective with an 84% contribution of the first 3^- one-phonon configuration and a two-phonon contribution of around 10%. The 3_2^- state remains a practically pure two-quasiparticle state. The third 3^- state is again more collective, but the main contribution is from the $[2_1^+ \times 3_1^-]$ two-phonon state. As mentioned earlier, the transition charge densities of two-phonon states are usually small. Therefore, the calculated transition charge density of the 3_3^- state, which is

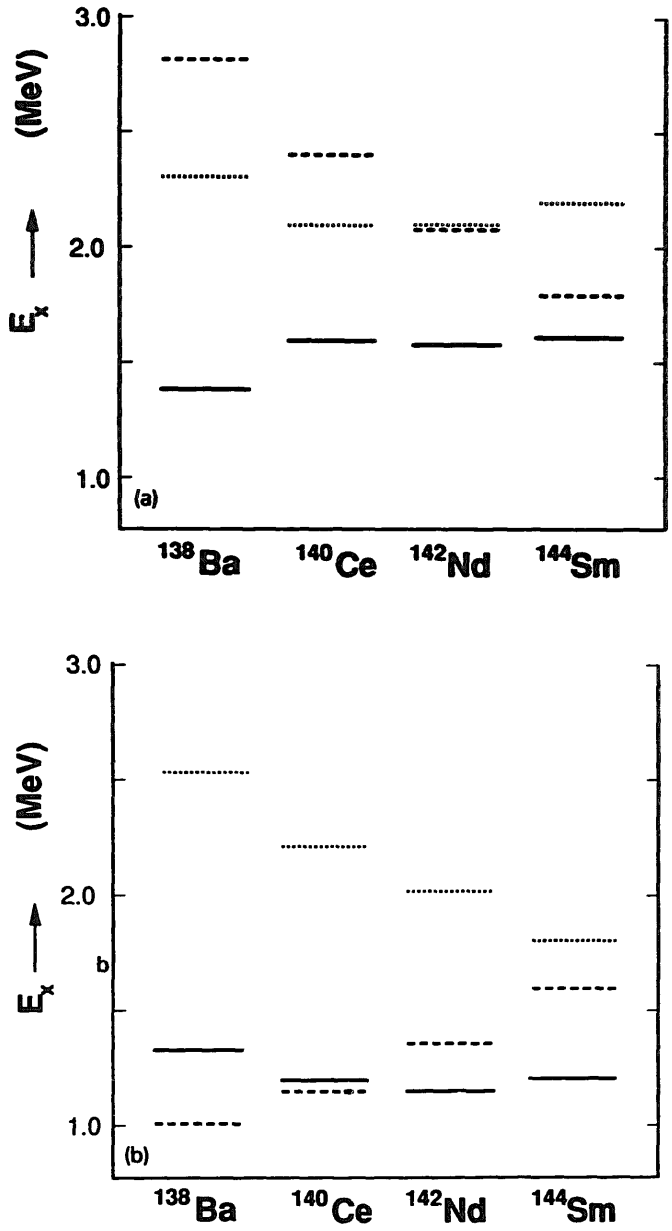

Fig. 6. (a) Experimental excitation energies of the 2_1^+ state (solid line), the 3_1^- state (dashed line) and the 4_1^+ state (dotted line) in the $N = 82$ even-A isotones from ^{138}Ba to ^{144}Sm. (b) Calculated energies of the $2d_{5/2}$ (solid line), $1g_{7/2}$ (dashed line) and $1h_{11/2}$ (dotted line) quasiparticle levels in the $N = 82$ even-A isotones from ^{138}Ba to ^{144}Sm.

shown in fig. 7 (together with the calculated and experimental ones of the 3_1^- state) is small.

Two octupole states have been observed in the present experiment, the first one at 2.083 MeV and the second one at 3.580 MeV. A transition charge density for the first state could not be extracted in a model-independent way because of the small difference in excitation energy of 15 keV between this state and the 4^+ state at 2.098 MeV. The experimental resolution was only good enough to resolve the peaks

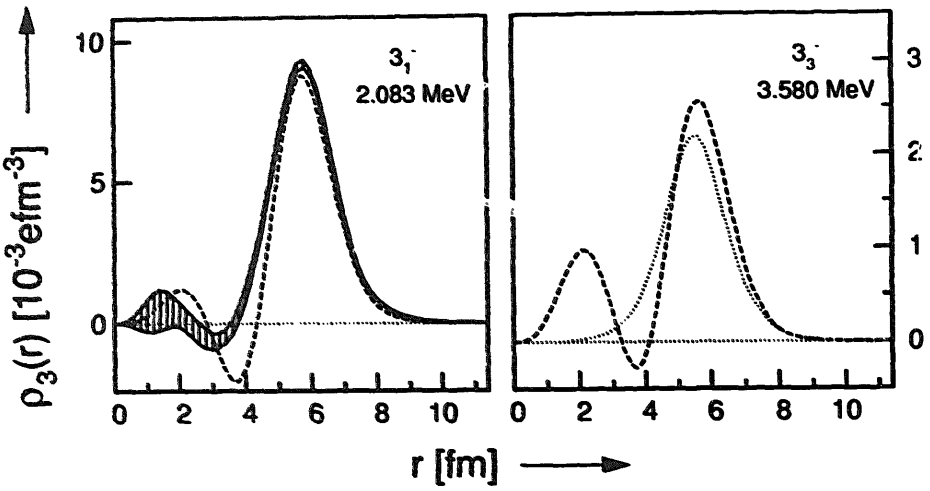

Fig. 7. The experimental transition charge density of the 3_1^- state at 2.083 MeV (curve with error band) compared to the results of the QPM calculations (dashed line) and the calculated transition charge density of the 3_3^- state at 3.580 MeV together with the standard density (dotted line) obtained from a fit to the data.

for momentum transfers up to 1.3 fm^{-1}. Therefore, a functional form assumed for the transition charge density of the weaker 4^+ state was substracted beyond 1.3 fm^{-1} from the form factor of the transition due to the excitation of both states.

The functional form chosen was the derivative of the ground-state charge density:

$$\rho_\lambda(r) = \mathrm{d}\rho_0(r)/\mathrm{d}r \tag{17}$$

with $\rho_0(r)$ being given by a three-parameter Fermi distribution. The parameters were taken from ref.[37]) and are used throughout this work, unless theoretical or other experimental evidence favours a different value for the average nuclear radius, which is in those cases clearly stated. This transition density is usually known as a one-phonon density. To avoid confusion, the name standard density will be used henceforward.

The validity of using a standard density for the 4_1^+ state will be discussed in the next section. The resulting - more or less - pure form factor for the 3_1^- state and the extracted transition charge density are shown in figs. 8 and 7, respectively. For the state at 3.580 MeV the diffraction pattern of the form factor at q-values beyond the first maximum is washed out because of contributions from other levels in this high level-density region. This made it impossible to obtain a transition charge density for this state. However, the position of the maximum of the form factor indicates that one is indeed dealing with an octupole state (see fig. 8). This confirmed by the already mentioned (p, p') experiment[5]). A B(E3) value for this state was extracted by assuming a transition charge density with a standard shape. This assumption is supported by the QPM calculations (see fig. 8), although for an optimal description of the experimental form factor the radius of the standard transition charge density had to be shifted to $r_0 = 5.5$ fm. The B(E3) values are listed in table 3.

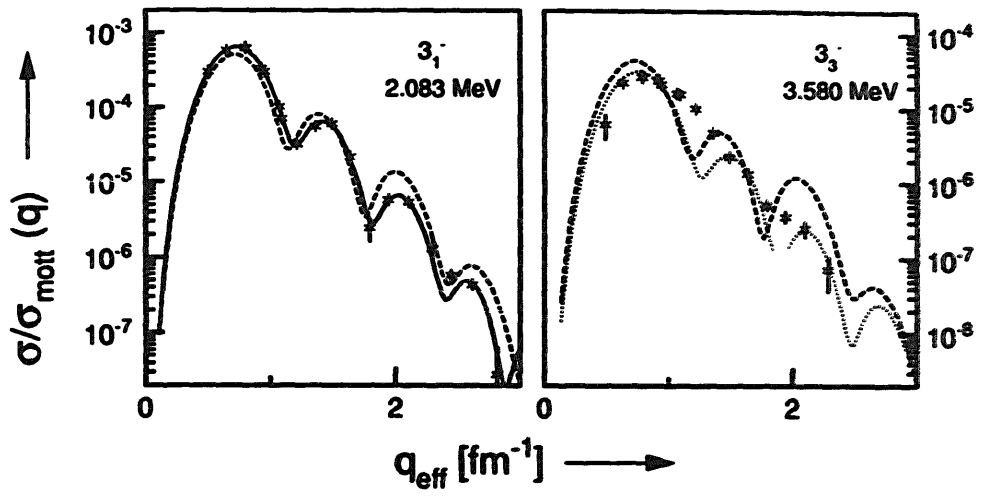

Fig. 8. Form factor data of the 3_1^- state at 2.083 MeV and the 3_3^- state at 3.580 MeV. The curves represent the fit obtained in a Fourier-Bessel analysis (solid line), the QPM calculation (dashed lines) and the fit using a standard density (dotted line).

4.3. HEXADECAPOLE STATES

Five hexadecapole one-phonon states are predicted by the RPA calculations below 4 MeV. Again, all one-phonon states are practically pure proton states. Table 4 lists the respective energies and B(E4) values. The 4_1^+ one-phonon state is much less collective than the 2_1^+ and the 3_1^- states, as the underlying configuration is for almost 90% of the two quasiparticle $(2d_{5/2}, 2d_{5/2})$ state. This confirms the findings of the (p, p') experiment by Trache *et al.* [5]), where the untypical angular distribution of the 4_1^+ state at 2.098 MeV is attributed to a large two-quasiparticle component. The 4_2^+ and 4_3^+ one-phonon states are also more or less pure two-quasiparticle states. However, the 4_4^+ one-phonon states, like the 2_4^+ state, is again quite collective with many two quasiparticle configurations contributing in a coherent way, which leads to a B(E4) value even larger than that of the 4_1^+ one-phonon state. Although many two-quasiparticle configurations contribute to the 4_5^+ state, some of them have a destructive interference, leading to a lower B(E4) value.

Coupling the one- and two-phonon states does not alter the first three hexadecapole states noticeably. Both the B(E4) values, shown in table 4, and the transition charge densities hardly change. However, the strength of the 4_4^+ one-phonon state at 3.628 MeV gets fragmented into two states, one at an excitation energy of 3.160 MeV, the other at 3.460 MeV. This is due to the coupling of the one-phonon state to the $[2_1^+ \times 2_1^+]$ two-phonon state at 3.8 MeV. Both states have a similar structure of approximately 40% of the 4_4^+ one phonon state, 40% of the mentioned two-phonon state and some 8% three-phonon contribution. The resulting states have therefore both a similar structure and strength.

In the present experiment five transitions were observed with a possible hexadecapole character; the form factors and the deduced transition charge densities

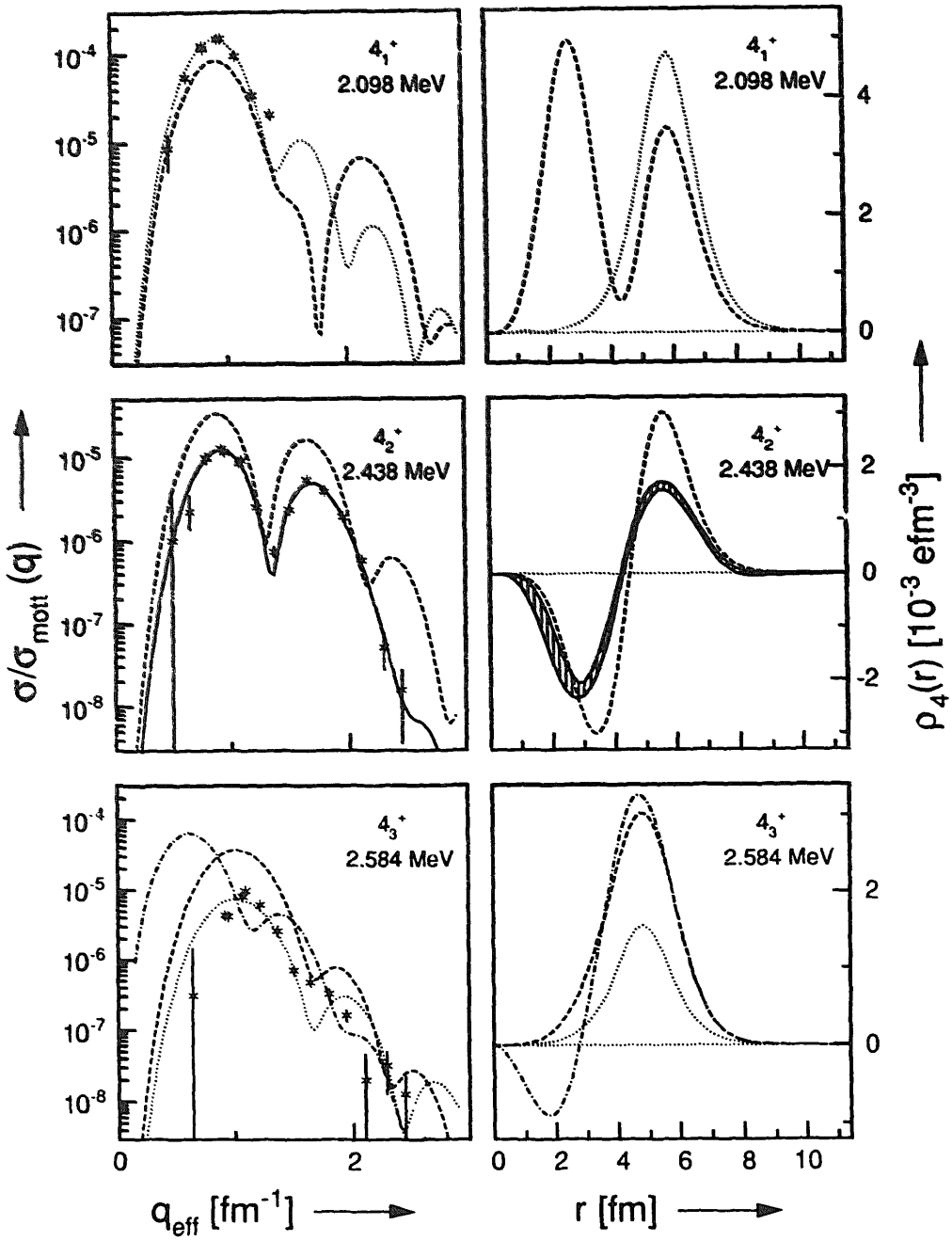

Fig. 9. Experimental form factor data with the fits obtained in a Fourier-Bessel analysis (solid lines) and deduced transition charge densities (curves with error bands) of the 4^+ states in ^{142}Nd. Dashed curves represent the form factors and transition charge densities of the QPM calculations and dotted curves the results of the respective fits with standard transition densities. In case of the 4_3^+ state the standard density is shifted to 4.8 fm. For the 4_3^+ state also a comparison with the QPM result for the 2_3^+ state is shown (dot-dashed curve).

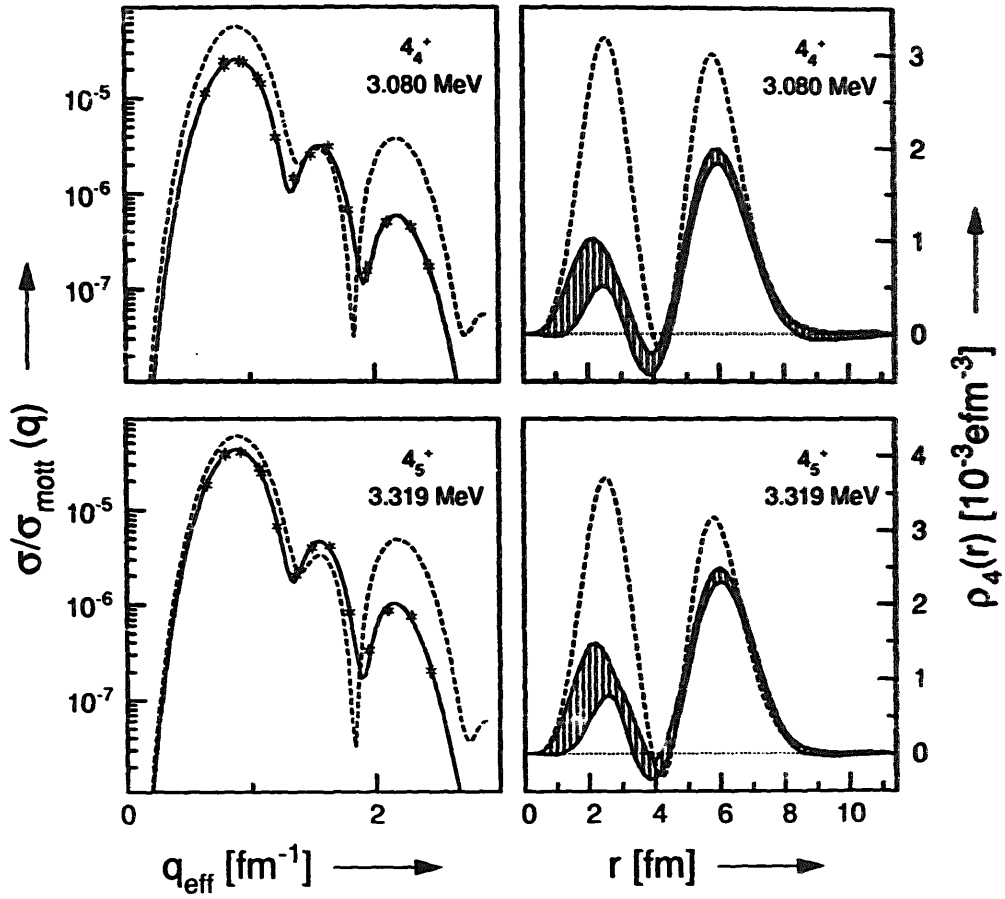

Fig. 9—continued

are depicted in fig. 9. The first state at 2.098 MeV has an excitation energy close to that of the 3_1^- state, as mentioned in the previous section. Therefore, only at the lowest incident energies was it possible to separate the peaks corresponding to the excitation of these levels and thus only the first maximum of the form factor of the 4_1^+ state up to 1.3 fm^{-1} is well determined. Clearly this range of momentum transfer is not large enough to extract a transition charge density.

The character of the level at 2.438 MeV is not known. The shape of the form factor permits two possible multipolarities, 0 or 4. However, we believe we are dealing with a 4^+ state for the following reasons:

(i) The level has not been observed in a (p, t) experiment by Ball *et al.* [38]), which was particularly sensitive for monopole excitations.

(ii) The level has been observed in the (p, p') experiment of Trache *et al.* [5]) and although no assignment was published, generally proton scattering is more sensitive to $\lambda = 4$ transitions than to $\lambda = 0$ transitions for angles larger than 30°.

(iii) The angular distribution of a state at 2.436 MeV, resulting from a preliminary analysis of the (p, p') experiment of Pignanelli *et al.* [32]), seems to indicate a 4^+ excitation.

TABLE 4

Excitation energies and B(E4) values of the hexadecapole states observed in this experiment compared to those from the QPM calculations. The results of the RPA calculations and those of the full calculations after coupling the two- and three-phonon states are listed

J^π	v	Calculation				Experiment	
		RPA		QPM			
		E_x (MeV)	B(E4) (e^2 fm^8)	E_x (MeV)	B(E4) (e^2 fm^8)	E_x (MeV)	B(E4) (e^2 fm^8)
4^+	1	2.280	17.3×10^5	2.160	19.5×10^5	2.098	41×10^5 [a]) 45×10^5 [b])
	2	2.480	6.5×10^5	2.430	7.8×10^5	2.438	$2.1\,(8)\times10^5$
	3	2.670	4.1×10^5	2.630	3.4×10^5	2.584	0.7×10^5 [c])
	4	3.630	34.7×10^5	3.160	14.8×10^5	3.080	$6.2\,(19)\times10^5$
	5	3.930	3.6×10^5	3.460	14.5×10^5	3.319	$11.4\,(17)\times10^5$
	6	4.030	0.8×10^5	3.700	2.2×10^5		
	7	4.080	0.2×10^5	3.990	0.5×10^5		

[a]) B(E4) using a standard density.
[b]) B(E4) using the QPM density.
[c]) B(E4) using a standard density shifted to $r = 4.8$ fm.

(iv) Both the systematics of the excitation energy and the structure of the transition charge density of the 4_2^+ state as predicted by the QPM agree very well with the experimental data for this transition as will be discussed below.

The level of 2.584 MeV has been given a $J^\pi = 1^{(+)}$ assignment in the literature [39]). However, both in the experiment of Trache *et al.* and in the present experiment a too large strength for this state is observed for it to have an unnatural parity. Therefore, it is assumed that another level with approximately the same energy is excited. The preliminary results of Pignanelli *et al.* give $J^\pi = 2^+$ for this state. However, based on the shape of the form factor as predicted by the QPM it is more likely to be the third hexadecapole state. Both possibilities will be discussed below.

The strong states at 3.080 MeV and 3.319 MeV are identified by Trache *et al.* as 4^+ states which is confirmed by the present work, since the shapes of both form factors are those of surface-peaked hexadecapole transitions and the magnitudes are consistent with the (p, p') experiment.

For the 4_2^+, 4_4^+ and 4_5^+ states, the agreement between the calculated and measured transition charge densities is rather good, both in structure and in strength, as is visible in fig. 9. However, the calculations predict too much strength in the nuclear interior for the latter two states. For the 4_1^+ state and the 4_3^+ state only a comparison on the level of form factors is possible, as shown in fig. 9. Concerning the 4_3^+ state it is clear that the position of the first maximum of the form factor is much better described by the transition charge density of the 4_3^+ state calculated in the QPM than by either that of the 2_3^+ state or that of a standard density peaking at the nuclear

surface. Since in general the overall structure of the transition charge densities is rather well predicted by the QPM, it strongly supports the conjecture, that the state at 2.584 MeV is a hexadecapole state. It must be mentioned though, that the experimental B(E4) value, listed in table 4, which was derived by making use of a standard transition density with its maximum shifted to 4.8 fm, is about a factor of three smaller than the one predicted by the QPM. The lack in strength and the position of the maximum of the transition charge density, located inside the nuclear interior, seems to explain why this state has not been identified before as the 4_3^+ state.

For the 4_1^+ state both the transition charge density of the QPM and the one with a standard density give a good fit to the first maximum of the form factor. The difference in the two calculated form factors is only visible beyond 1.4 fm^{-1}, where no data are available. Therefore, in table 4 two B(E4) values are listed. However, we believe that the description of the standard density is more realistic than that of the QPM. A clue to this can be obtained from the experimental transition charge densities of the 4_1^+ states in ^{142}Ce [ref. [3])] and ^{144}Nd [ref. [40])]. In either nucleus the extraction of the transition charge density is not hampered by other strongly excited states and form factors were obtained up to 2.15 fm^{-1}. The obtained transition charge densities for the 4_1^+ states showed very little structure in the nuclear interior. The calculations for these nuclei in the framework of the QPM [refs. [40,41])], however, predict a similar structure for these states as in ^{142}Nd. They are more or less pure $(2d_{5/2}, 2d_{5/2})$ two-quasiparticle states and their structure in the nuclear interior is also overestimated. This was also the case for the 2_1^+ state in ^{142}Nd (see sect. 4.1).

For all of the mentioned states this discrepancy can be traced back to a too large contribution of the $(2d_{5/2}, 2d_{5/2})$ configuration in the calculations, of which the transition charge density, shown in fig. 10, has a maximum at 2.8 fm^{-1}. This contribution can be reduced by adjusting the spin-orbit part of the potential used to calculate the single-particle spectrum which thus brings the $1g_{7/2}$ and $2d_{5/2}$ levels closer

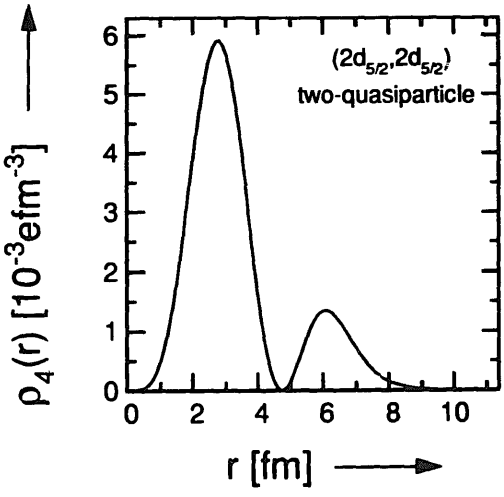

Fig. 10. Calculated hexadecapole transition charge density of the $(2d_{5/2}, 2d_{5/2})$ two-quasiparticle configuration.

together. This would lead to an enhancement of the $(2d_{5/2},1g_{7/2})$ component in the 4_1^+ one-phonon state and a better agreement with the experimental transition charge densities. However, this would mean an *ad hoc* adjustment of parameters, as neither accurate experimental data on the spin-orbit term are available to justify this adjustment, nor is the QPM, or any other model for that matter, sufficiently accurate to determine single-particle energies in neighbouring odd nuclei. Thus, the origin of the large structure in the interior of the nucleus for the 2_1^+ state and the 4_1^+ state is understood, but on theoretical grounds there is as yet no reason to adjust parameters to obtain better agreement with the experiment.

4.4. OTHER MULTIPOLARITIES

Monopole states - Only two excited 0^+ states in ^{142}Nd below an excitation energy of 3 MeV are reported in the literature; the rather weakly excited 0_2^+ state at 2.217 MeV and the strongly excited 0_3^+ state at 2.978 MeV [ref. [38])]. For the 0_3^+ state a transition charge density, depicted in fig. 11, was obtained with the typical shape of a density vibration. The B(E0) value is listed in table 5, As in the QPM particle-particle correlations were not taken into account in the residual interaction, the description of the monopole states is expected to be incomplete. Hence, no comparison with a calculated transition charge density has been performed.

The excitation energy of the 0_2^+ state is only 10 keV apart from the 6_1^+ state at 2.206 MeV, making it impossible to resolve these states. As the form factor of the doublet has a first maximum at 1.15 fm^{-1}, a value considerably larger than the 1.0 fm^{-1} of the state at 2.976 MeV, it seems unlikely that the observed transition, if it were due to a monopole state, constitutes a typical density vibration. Therefore, it has been treated as as a pure 6^+ transition.

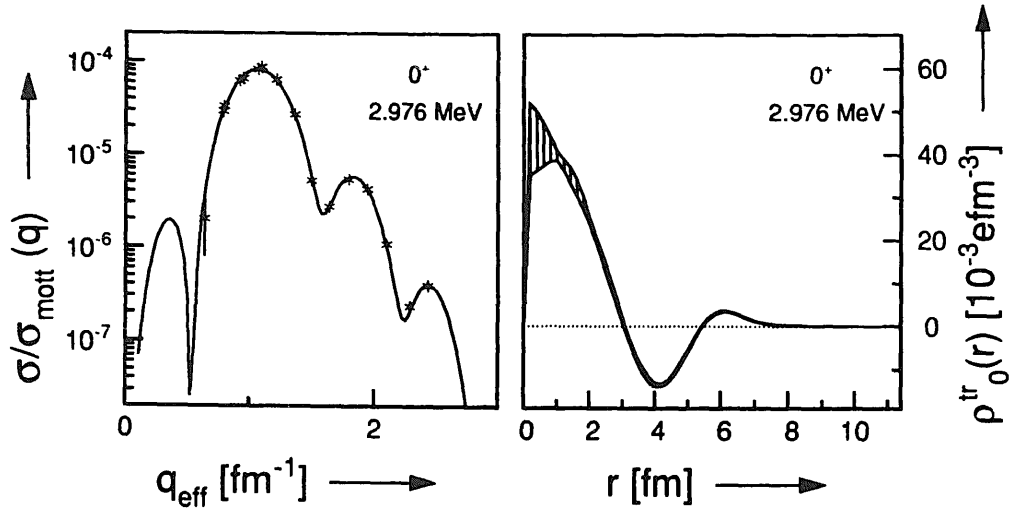

Fig. 11. Experimental form-factor data with the Fourier-Bessel fit and deduced transition charge density of the 0^+ state at 2.976 MeV.

TABLE 5

Excitation energies and $B(E\lambda)$ values of the remaining states observed in this experiment compared to those from the QPM calculations. The results of the RPA calculations and those of the full calculations after coupling the two- and three-phonon states are listed

J^π	v	Calculation				Experiment	
		RPA		QPM			
		E_x (MeV)	$B(E\lambda)$ (e^2 fm$^{2\lambda}$)	E_x (MeV)	$B(E\lambda)$ (e^2 fm$^{2\lambda}$)	E_x (MeV)	$B(E\lambda)$ (e^2 fm$^{2\lambda}$)
0^+						2.976	88 (41) [a]
1^-	1	7.140	1.38×10^{-5}	3.790	2.15×10^{-4}	3.425 [b]	$1.83\,(39)\times10^{-2}$ [b]
5^-	1	3.000	1.74×10^{8}	2.670	1.58×10^{8}	2.739	$1.21\,(12)\times10^{8}$
	2	3.340	0.10×10^{8}	3.250	0.19×10^{8}		
	3	4.580	0.75×10^{8}	3.840	0.95×10^{6}		
6^+	1	2.300	8.63×10^{9}	2.210	8.61×10^{9}	2.206	$9.4\,(20)\times10^{9}$
	2	2.690	0.15×10^{9}	2.650	0.85×10^{9}	2.893	8×10^{7} [c]
	3	3.990	2.35×10^{9}	3.730	2.26×10^{9}	3.413	2×10^{9} [d]
7^-	1	3.160	1.48×10^{11}	2.920	1.35×10^{11}	3.246	$2.5\,(4)\times10^{11}$
	2	3.340	0.65×10^{11}	3.250	0.75×10^{11}		
8^+	1	4.040	2.00×10^{12}	3.870	1.72×10^{12}		
9^-	2	3.310	5.42×10^{14}	3.210	5.13×10^{14}	3.494	2×10^{15} [d]

[a]) In units of e^2 fm^4.
[b]) This state has not been observed in the present experiment. The $B(E1)$ value is from Pitz *et al.* [6]).
[c]) $B(E\lambda)$ obtained using a standard density with a maximum at $r = 4.7$ fm.
[d]) $B(E\lambda)$ obtained using a standard density.

Dipole states - The QPM predicts the first one-phonon 1^- state at an excitation energy above 7 MeV. There is, however, a dipole two-phonon state with the $[2_1^+ \times 3_1^-]$ structure at approximately 3.7 MeV. Although this state has been observed as quite a strong excitation in a photon scattering experiment [6]) at 3.425 MeV with a $B(E1)$ value of $18.3 \pm 3.9 \times 10^{-3}$ e^2 fm^2, it has not been observed in the present experiment. Photon scattering probes the isovector dipole character of the state at the $q = \omega$ photon point, whereas in the measured q-range electron scattering is sensitive to the isoscalar charge density which is probably small due to the two-phonon character of this state (see also fig. 4).

High multipolarity states - For the 5^- and higher multipolarity states the description within the QPM has its shortcomings. This has several reasons. First, in the calculation of the single-particle spectrum only bound and narrow quasi-bound states are included. This approximation of not including the continuum is too crude for high multipolarity states. An indication of this is obtained if one looks at the exhaustion of the energy-weighted sum rule (EWSR) [30]) for the different multipolarities. Whereas for the multipolarities up to 3^- the EWSR is exhausted for more than 80%, this number gradually decreases for the states of high multipolarity. The calculated numbers are listed in table 6. Second, it is difficult to investigate the validity of

TABLE 6

The exhaustion of the respective energy-weighted sum rules (EWSR) by the states predicted by the QPM for the different multipolarities, for the model basis discussed in the text

J^π	1^-	2^+	3^-	4^+	5^-	6^+	7^-	8^+	9^-
EWSR (%)	94.6	95.0	79.7	65.6	61.5	50.4	44.1	47.6	39.1

keeping the strength ratio for the isovector to isoscalar forces constant, as for many nuclei the isovector counterparts of the isoscalar states have not been identified yet. Third, the parameters $\kappa_0^{J^\pi}$ are adjusted to reproduce the excitation energy and collectivity of the low-lying states, which are mainly built from a single one-phonon state. However, the high-multipolarity states are not collective and contain significant admixtures of two- and three-phonon components, thus making their excitation energy more sensitive to the single quasi-particle level scheme than to the parameters $\kappa_0^{J^\pi}$. Indeed, if the isoscalar force $\kappa_0^{J^\pi}$ is adjusted for the excitation energy of the first state of each multipolarity to coincide with that of the experiment, unrealistic values are obtained for this parameter. Therefore, another procedure was chosen for $\lambda \geq 5$. The multipole strength term for the negative-parity states was set at that of the octupole states, whereas that of the positive-parity states was set at that of the quadrupole states. Hence, *a priori* one should expect only a schematic agreement with the experiment.

In the present experiment six states of high multipolarity were identified with reasonable certainty. First, the level at 2.206 MeV, which is a superposition of the 0_2^+ state and the 6_1^+ state, has been treated as a pure 6^+ transition (see also the section on the monopole states). The transition charge density extracted as such is shown in fig. 12. Furthermore, two other possible 6^+ states were found at excitation energies of 2.893 and 3.413 MeV. However, because of the weakness of the states and the filling of the form factor minima, possibly due to admixtures of other states, only the form factors are shown in fig. 12. A B(E6) value for these states was determined using a standard shape, according to the prescription discussed earlier. The same procedure was followed for the state at 3.494 MeV, which is assumed to be a 9^- state (see also fig. 13).

The remaining states of high multipolarity for which it was possible to obtain transition charge densities are the 5^- state at 2.739 MeV and the 7^- state at 3.246 MeV, shown in fig. 14. The multipolarities for all of the mentioned states were determined on the basis of the position of the first maximum of the form factor, assuming a surface-peaked transition charge density. All the obtained $B(\mathrm{E}\lambda)$ values are listed in table 5.

5. Summary and conclusions

An (e, e') experiment has been performed on the semi-magic ($N = 82$) nucleus ^{142}Nd for momentum transfers up to 2.8 fm^{-1}. The excellent energy resolution made

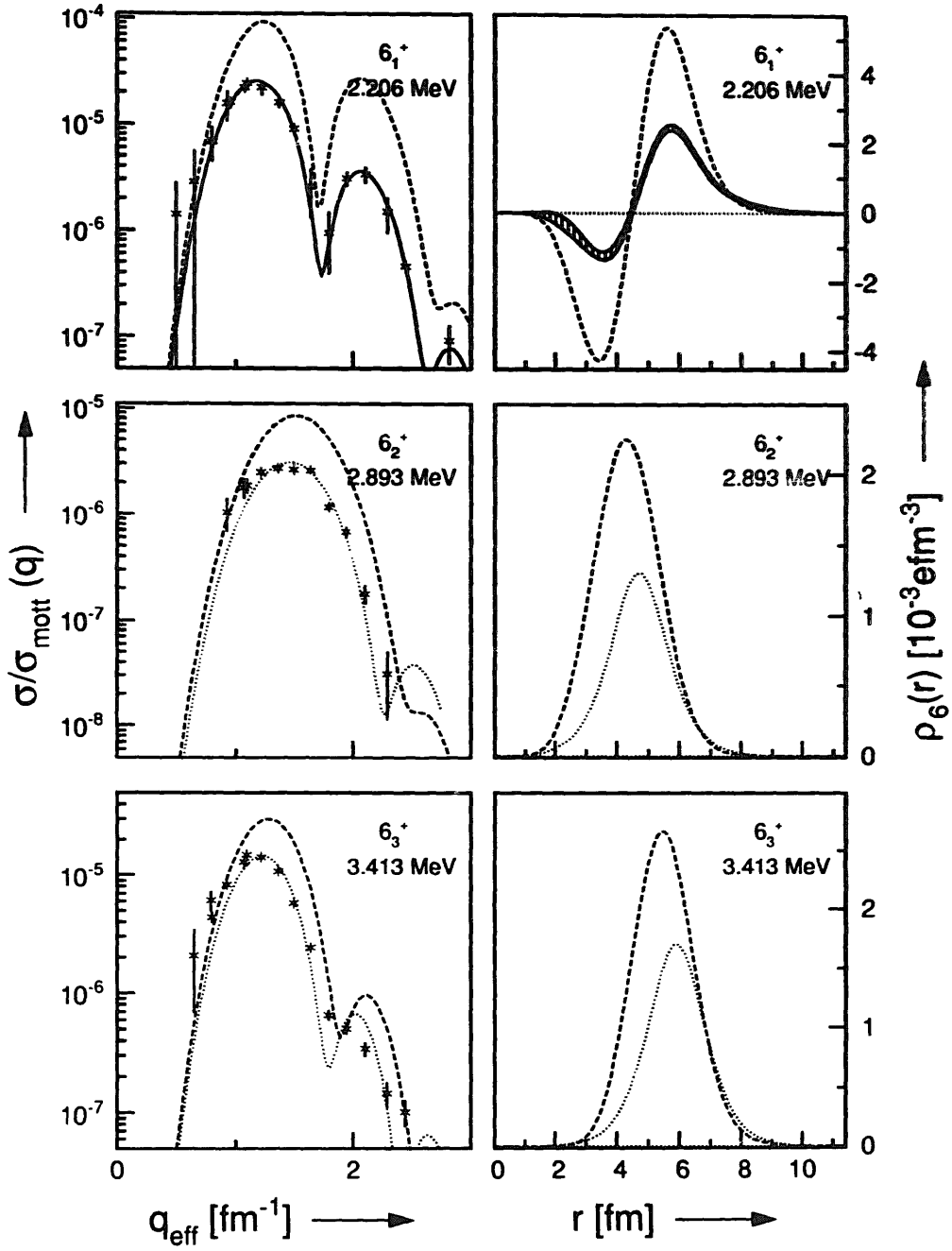

Fig. 12. Experimental form-factor data of the 6_1^+ state at 2.206 MeV, the 6_2^+ state at 2.893 MeV and the 6_3^+ state at 3.413 MeV. The solid line represents the Fourier-Bessel fit, the dashed lines the QPM calculations, and the dotted lines the form factors obtained from the standard transition density. Also drawn are the experimental (curve with error band), the QPM (dashed lines) and the standard (dotted lines) transition charge densities of the respective states. For the 6_2^+ state and the standard transition density has been shifted inward to fit the form-factor data.

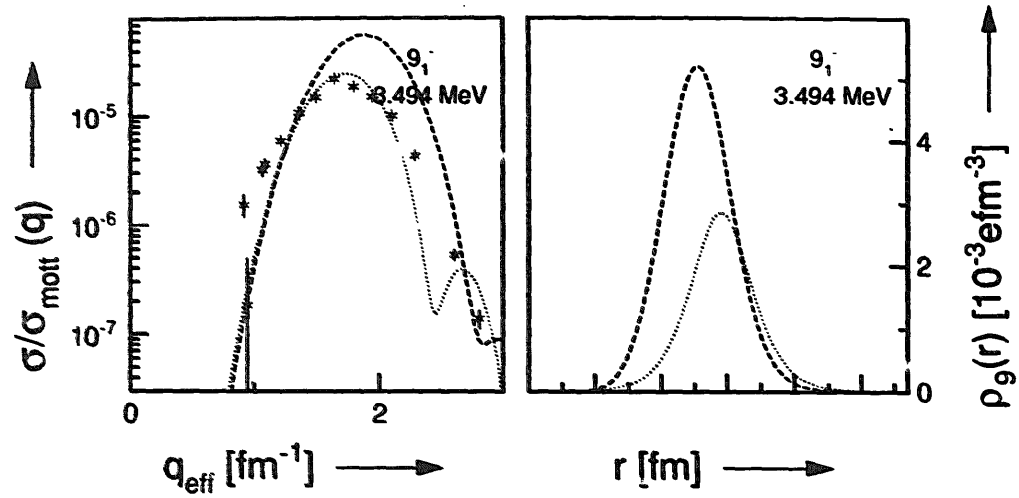

Fig. 13. Experimental form-factor data of the 9_1^- state at 3.494 MeV in comparison with the QPM calculations (dashed line) and the fit obtained with a standard transition density (dotted line). Also shown are the QPM and standard transition charge densities.

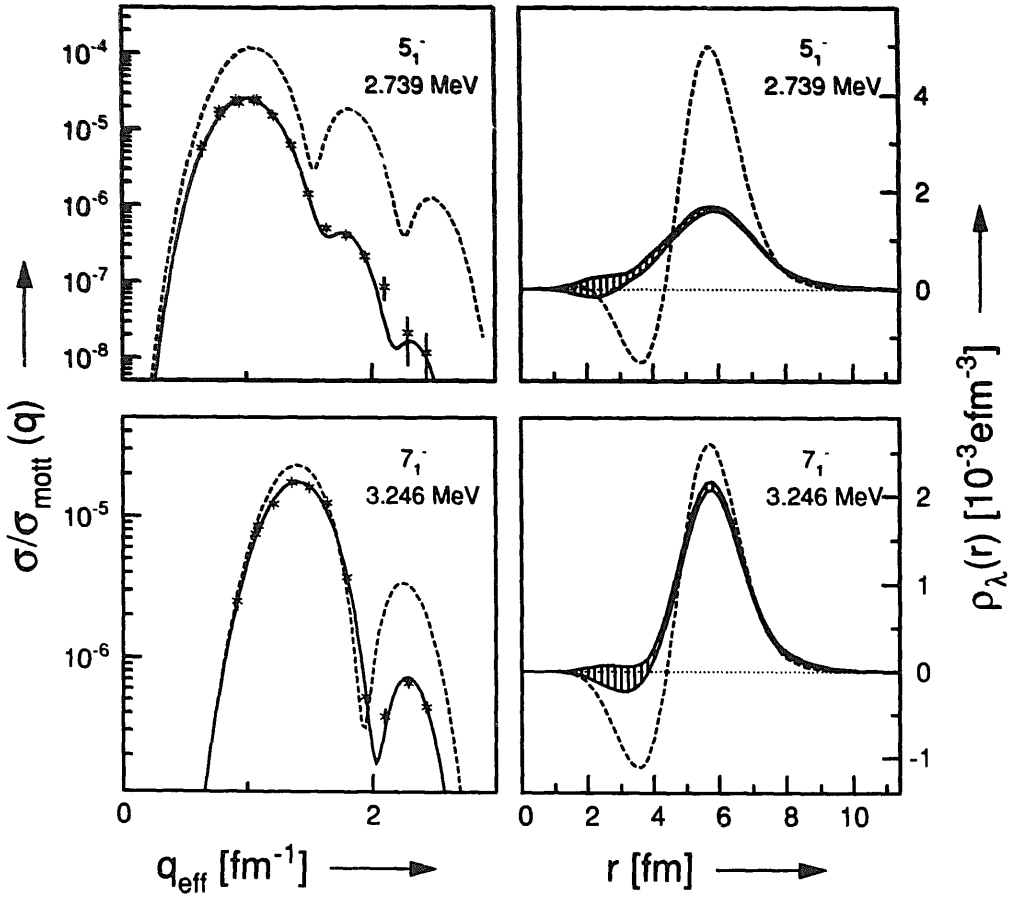

Fig. 14. Experimental form-factor data of the 5_1^- state at 2.739 MeV and the 7_1^- state at 3.246 MeV with the respective transition charge densities (curves with error band). The solid lines represent the Fourier-Bessel fits and the dashed lines the results from the QPM calculations.

it possible to identify many transitions of different multipolarities up to an excitation energy of 3.7 MeV. Some new levels have been observed, like the 4^+ state at 2.438 MeV, the 5^- state at 2.739 MeV and the 6^+ state at 2.893 MeV. Also several levels found in other experiments have been confirmed and for some of these levels a multipolarity has been suggested. For many of these states accurate transition charge densities were obtained by means of a Fourier–Bessel analysis of measured form factors. In cases where this was not possible due to a limited q-range in which form factors were measured, $B(E\lambda)$ values were determined by assuming a surface-peaked transition charge density. The diversity of the data – multipolarities from 0 up to 9, identification of three quadrupole and four hexadecapole states – allows a systematic investigation of the modes of excitation of these low-lying states. Special attention has been given in this respect to the interplay between single-particle and collective degrees of freedom. To this end, the experimental results were compared with calculations in the framework of the quasiparticle–phonon model (QPM).

The QPM is a microscopic model in which the calculations are performed in two steps. First, basis states called "phonons" are generated, whereby phonons are defined as both collective and non-collective solutions of the BCS quasiparticle RPA equations. Second, two- and three-phonon states are constructed and simultaneously the coupling between these states is included. In this way one accounts for pairing interactions as well as multipole correlations. The proton part of the radial parameters of the Saxon–Woods potential used in the calculations have been taken from the results of an (e, e'p) experiment on ^{142}Nd, performed at the NIKHEF [28]). These new parameters lead to a much better description of the radial dependence of the transition charge densities than the parameters used before [7]).

In general, the agreement between the experimental data and the calculations is quite reasonable. The systematics of the excitation energies and $B(E\lambda)$ values as well as the structure of the transition charge densities are well described by the calculations. The predictions for the quadrupole states and the hexadecapole states are especially interesting in view of the many experimental transition charge densities obtained for such states. Indeed, all characteristic features of the mentioned states are at least qualitatively described, such as for example the degree of collectivity of the quadrupole states: the 2_1^+ and 2_4^+ states being collective, in contrast to the 2_2^+ and 2_3^+ states. A possible explanation is found in the underlying subshell structure of the nucleus, especially the gap of approximately 2 MeV between the single-particle energies of the $2d_{5/1}$ and $1g_{7/2}$ subshells on the one hand and the $1h_{11/2}$, $2d_{3/2}$ and $3s_{1/2}$ subshells on the other hand. A similarly contrasting behaviour is seen in the transition charge densities, that of the 2_2^+ state showing a pronounced volume peak whereas those of the 2_1^+ and 2_4^+ states are mainly surface peaked. This has been explained to arise from both the coupling of the one-phonon states to the multiple-phonon states and the structure of the one-phonon states. Also the reason why the 2_3^+ state is not observed in the present experiment could be understood.

The situation for the hexadecapole states is quite different. The 4_1^+ state is calculated to be an almost pure two-quasiparticle state. Although experimentally

this state could not be separated from the much stronger 3_1^- state for momentum transfers higher than 1.3 fm^{-1}, thus making it impossible to extract a transition charge density, the experimental B(E4) values assuming a standard shape (i.e. the derivative of the ground-state charge density) are found to be in reasonable agreement with the calculations. The two-quasiparticle character of this transition has also been suggested by ref. [5]) on the basis of an anomalous angular distribution in a (p, p') experiment. The state at 2.438 MeV has been observed before [5]), but no spin or parity could be assigned. We propose it as a candidate for the 4_2^+ state. Indeed, the transition charge density, assuming a 4^+ transition, is in good agreement with the calculations. The 4_3^+ state, calculated to be by far the weakest hexadecapole state up to 4 MeV, might be the state seen at 2.584 MeV. The 4_4^+ and 4_5^+ states have been observed by Trache *et al.* [5]) and are confirmed by the present experiment. Both the B(E4) values and the structures are in reasonable agreement with the calculations. It is worth noting that the two-phonon admixture is large and up to 50% for these states.

The description of the underlying configurations which contribute in the excitation of the 3_1^- state, the only octupole state for which a transition charge density could be extracted, has led to an intuitive explanation for the strong proton number dependence of the excitation energy of this state within the even $N = 82$ isotones. In contrast to the 2_1^+ and 4_1^+ states, which are mainly built from excitations within a subshell, the configurations that contribute to the 3_1^- state are by necessity excitations from one subshell to another, thus making this level more sensitive to the relative excitation energies of the different subshells. It is shown that the single-particle energy spacing between the $2d_{5/2}$, $1g_{7/2}$ and the $1h_{11/2}$ indeed depends rather strongly on the proton number in going from ^{138}Ba to ^{144}Sm.

For the states of higher multipolarity only a qualitative agreement between the experimental data and the calculations is obtained. This has two reasons: first, the quality of the data for these states is generally not good enough to extract transition charge densities. Therefore only B(Eλ) values are obtained, again assuming a standard shape. Second, the theory does not pretend to describe noncollective high-multipolarity states as well as collective ones. Moreover, the isoscalar strength term of the residual interaction was taken for the positive-parity states to be the same as for the quadrupole states, whereas the value for the negative-parity states was the same as for the octupole states. For three states, i.e. the 6^+ at 2.206 MeV, the 5^- at 2.739 MeV and the 7^- at 3.246 MeV, experimental transition charge densities were obtained and compared with the calculations yielding qualitative agreement. For other states, notably the 6^+ states at 2.893 MeV and 3.413 MeV and the 9^- state at 3.494 MeV the comparison between the calculation and the experiment was only possible at the level of form factors.

As monopole states cannot be described in a consistent way without the inclusion of the particle-particle channel in the residual interaction, only the experimental data are shown for the state at 2.976 MeV. Concerning the dipole states, the first

1^- state is known to have an excitation energy of 3.425 MeV. This state is the $[2_1^+ \times 3_1^-]$ two-phonon state, and in general two-phonon states have small transition charge densities. Indeed, this excited state has not been observed in the present experiment.

The authors would like to thank M. Pignanelli and R. De Leo for furnishing their recent (p, p') data prior to publication. One of the authors (V.P.) would like to thank M. Grinberg, Ch. Stoyanov and V.V. Voronov for many fruitful discussions. Moreover, he would like to thank the Free University of Amsterdam and NIKHEF-K for their hospitality during the visit when this paper was completed.

This work is part of the research program of the Foundation for Fundamental Research of Matter (FOM), which is financially supported by the Netherlands' Organisation for Scientific Research (NWO).

References

1) V. Meot, PhD Thesis, University of Paris VII (1987), unpublished
2) X.-H. Phan, H.G. Andresen, L.S. Cardman, J.-M. Cavedon, J.-C. Clemens, B. Frois, M. Girod, D. Gogny, B. Grammaticos, R. Hoffmann, M. Huet, P. Leconte, S.K. Platchkov, I. Sick and S.E. Williamson, Phys. Rev. **C38** (1988) 1173
3) W.Y. Kim, private communication (1990)
4) O. Schwentker, J. Dawson, J. Robb, J. Heisenberg, J. Lichtenstadt, C.N. Papanicolas, J. Wise, J.S. McCarthy, L.T. van der Bijl and H.P. Blok, Phys. Rev. Lett. **50** (1983) 15
5) L. Trache, J. Wrzesinski, C. Wesselborg, A. Clauberg, K.O. Zell, R. Reinhardt, P. von Bretano, D. Bazacco, G.P.A. Berg, W. Hürlimann, J. Meissburger and J.L. Tain, Nucl. Phys. **A492** (1989) 23
6) H.H. Pitz, R.D. Heil, S. Lindenstruth, I. Seemann, R. Stock, C. Wesselborg, A. Zilges, P. von Bretano, S.D. Hoblit and A.M. Nathan, Nucl. Phys. **A509** (1990) 587
7) R.K.J. Sandor, H.P. Blok, U. Garg, M.N. Harakeh, C.W. de Jager, V.Yu. Ponomarev, A.I. Vdovin and H. de Vries, Phys. Lett. **B233** (1989) 54
8) C. de Vries, C.W. de Jager, L. Lapikás, G. Luijcks, R. Maas, H. de Vries and P.K.A. de Witt Huberts, Nucl. Instr. Meth. **233** (1984) 1
9) J.H.J. Distelbrink, E. Kok, H. Blok, J.L. Visschers and P.K.A. de Witt Huberts, Nucl. Instr. Meth. **220** (1984) 433
10) H. Blok, E.A.J.M. Offerman, C.W. de Jager and H. de Vries, Nucl. Instr. Meth. **A262** (1987) 291
11) A.J.C. Burghardt and W.T.A. Borghols, NIKHEF-K, internal report 84-A2 (1984), unpublished
12) E.A.J.M. Offerman, PhD Thesis, University of Amsterdam (1988), unpublished
13) C.E. Hyde-Wright, PhD Thesis, MIT (1984), unpublished
14) L. Maximon, Rev. Mod. Phys. **41** (1969) 193
15) E.A.J.M. Offermann, L.S. Cardman, C.W. de Jager, H. Miska, C. de Vries and H. de Vries, Phys. Rev. C, submitted for publication
16) J. Heisenberg, Adv. Nucl. Phys. **12** (1981) 61
17) J. Heisenberg and H.P. Blok, Ann. Rev. Nucl. Part. Sci. **33** (1983) 596
18) H. Rothhaas, J. Friedrich, K. Merle and B. Dreher, Phys. Lett. **B51** (1974) 23
19) I. Sick, Phys. Lett. **B116** (1982) 212
20) S. Galès, Ch. Stoyanov and A.I. Vdovin, Phys. Reports **166** (1988) 125
21) L.A. Malov and V.G. Soloviev, Sov. J. Part. Nucl. **11** (1980) 301
22) V.V. Voronov, Nguen Din Dang, V.Yu. Ponomarev, V.G. Soloviev and Ch. Stoyanov, Sov. J. Nucl. Phys. **40** (1984) 438
23) V.G. Soloviev, Progr. Part. Nucl. Phys. **19** (1987) 107
24) V.V. Voronov and V.G. Soloviev, Sov. J. Part. Nucl. **14** (1983) 583

25) V.G. Soloviev, Ch. Stoyanov and R. Nikolaeva, Bull. Acad. Sci. USSR, Phys. Ser. 47 (1983) 2082
26) H.C. Lee, Preprint of Chalk River Nuclear Laboratories, AECL-4839, Chalk River, Ontario (1975)
27) G.G. Simon, C. Schmitt, F. Borkowski and V.H. Walther, Nucl. Phys. A333 (1980) 381
28) J.B.J.M. Lanen, PhD Thesis, University of Utrecht (1990), unpublished
29) V. Yu. Ponomarev, V.G. Soloviev, Ch. Stoyanov and A.I. Vdovin, Nucl. Phys. A323 (1979) 446
30) A.M. Bernstein, Adv. Nucl. Phys., vol. 3, ed M. Baranger and E. Vogt (Plenum, New York, 1969) p. 321
31) L.K. Peker, Nucl. Data Sheets 43 (1984) 579
32) M. Pignanelli and R. De Leo, private communication (1990)
33) A.I. Vdovin and Ch. Stoyanov, Bull. Acad. Sci. USSR, Phys. Ser. 38 (1974) 119
34) D.T. Khoa, I.N. Kukhtina and V.Yu. Ponomarev, Sov. J. Nucl. Phys. 44 (1986) 585
35) W.P. Jones, L.P. Borgman, K.T. Hecht, J. Bardwick and W.C. Parkinson, Phys. Rev. C4 (1971) 580
36) A.I. Vdovin *et al.*, to be published
37) J.H. Heisenberg, J.S. McCarthy, I. Sick and M.R. Yearian, Nucl. Phys. A164 (1971) 340
38) J.B. Ball, R.L. Auble, J. Rapaport and C.B. Fulmer, Phys. Lett. B30 (1969) 533
39) J. Tenenbaum, R. Moret and A. Nof, Nucl. Phys. A218 (1974) 95
40) J. Mieremet, Masters Thesis, University of Amsterdam (1990), unpublished
41) V.Yu. Ponomarev *et al.*, to be published